ISSN 0038-0946, Solar System Research, 2010, Vol. 44, No. 3, pp. 223–237. © Pleiades Publishing, Inc., 2010.
Original Russian Text © M.Yu. Reshetnyak, 2010, published in Astronomicheskii Vestnik, 2010, Vol. 44, No. 3, pp. 244–258.

Convection and Heat Exchange during Rapid Rotation

M. Yu. Reshetnyak

Schmidt Joint Institute of Physics of the Earth, Russian Academy of Sciences, Bol'shaya Gruzinskaya ul. 10, Moscow, 123810 Russia

Received November 26, 2008

Abstract—Convection is highly geostrophic in the liquid cores of planets. A three-dimensional Boussinesq model in a plane rotating layer is considered in this study, and an analysis is given of the mechanism of the nonlinear interaction of Fourier waves that results in energy transfer through the spectrum. The structure of the wave triangle is demonstrated to be strongly different on scales smaller (or larger) than those of the leading mode of cyclonic turbulence. The differences in the structure of the triads of the thermal turbulence from that in the Kolmogorov model of homogeneous and isotropic turbulence are shown. The regimes with rotation considered in the study are typical of the modern models of convection and dynamo in the cores of planets, including the Earth.

DOI: 10.1134/S0038094610030056

INTRODUCTION

A large number of studies on magnetic-field generation in the cores of planets and their satellites have appeared since the mid-1990s (see references in (Jones, 2000)). In the pioneering works, only the principal possibility of magnetic-field generation was examined using simple Boussinesq models of thermal convection in a sphere (Glatzmaier and Roberts, 1995). Later, the studies focused on the properties of the generated magnetic field in their dependence on the parameters of diffusion coefficients, the amplitude of heat sources, material differentiation, the types of boundary conditions, the solid core effects, and many other parameters (Christensen et al., 1999). A variety of numerical three-dimensional dynamo models in a sphere has been developed so far. They can reproduce both axisymmetric magnetic fields, such as geomagnetic ones, and fields generated by magnetic dipoles, tending to the equatorial plane for giant planets (Stanley and Bloxham, 2004). However, the validity of the coefficients of turbulent transfer used in all of the dynamo and convection models (without any exception) is still an open question. For the Earth's core, simple estimates based on the western-drift amplitude give the Reynolds number $\mathrm{Re} \sim 10^9$, thus immediately showing that the problem cannot be solved using state-of-the-art supercomputers. The situation is generally the same for the other planets in which the dynamo process is possible. The magnetic Reynolds number $\mathrm{R_m}$ is estimated at 10^2 to 10^3, which is already suitable for the present computer facilities. Thus, on one hand, the basic problem of the modern models of planetary dynamo is a correct description of hydrodynamics. On the other hand, we cannot apply such well-known turbulence models as those of Prandtl, Smagorinsky, and $k - \varepsilon$, because the anisotropy related to the fast diurnal rotation in planetary cores can reach several orders of magnitude. At the same time, from the standpoint of an observer on the planetary surface, the magnetic-field structure and the integral spectrum may only weakly depend on the abovementioned parameters and the applied turbulence model. In this sense, the problem of planetary dynamo is ill-posed. It seems reasonable to preliminarily investigate the statistical properties of turbulence both in physical and wave spaces in order to correctly determine the turbulence coefficients in large-scale equations. Although large volumes of information about the inner structure of planets and satellites have been recently accumulated (Zharkov, 2003), the solution to this problem is complicated even for simple Boussinesq-type models. The estimates given below show that the flux analysis in the wave space turns out to be more important in cases when the systems cannot be differentiated by other parameters. The examination of fluxes in the wave space (in other words, the redistribution of some variables between scales) is closely related to the structure of the wave triangle during a nonlinear interaction and the role of rotation in this process. This is also examined below.

CONVECTION EQUATIONS

Let us consider the thermal convection of an incompressible liquid $\nabla \cdot \mathbf{V} = 0$ in a rectangular box, rotating with an angular velocity Ω about the vertical axis $\mathbf{z}$. Let us assume that the velocity $\mathbf{V}$, the time t, and the pressure P are, respectively, measured in units of κ/L, L^2/κ and $\rho\kappa^2/L^2$, where L is the unit of length,

κ is the thermal diffusivity, and ρ is the material density. Then, the dynamo equations in the Cartesian system of coordinates (x,y,z) can be written in the following form:

$$\begin{aligned} &\mathrm{E}\,\mathrm{Pr}^{-1}\left[\frac{\partial \mathbf{V}}{\partial t} - \mathbf{V}\times(\nabla\times\mathbf{V})\right] \\ &= -\nabla P - 1_z\times\mathbf{V} + \mathrm{Ra}\,T\,1_z + \mathrm{E}\Delta\mathbf{V} \\ &\frac{\partial T}{\partial t} + (\mathbf{V}\cdot\nabla)(T+T_0) = \Delta T. \end{aligned} \quad (1)$$

The dimensionless Prandtl, Ekman, and modified Rayleigh and Roberts numbers are introduced as follows: $\mathrm{Pr} = \frac{\nu}{\kappa}$, $\mathrm{E} = \frac{\nu}{2\Omega L^2}$ and $\mathrm{Ra} = \frac{\alpha g_0 \delta T L}{2\Omega\kappa}$, where ν is the kinematic viscosity coefficient, α is the coefficient of volume expansion, g_0 is the gravitational acceleration, δT is the unit of temperature T perturbation with respect to the "diffusive" temperature distribution $T_0 = 1 - z$, η is the magnetic diffusivity. We define the Rossby number as $\mathrm{Ro} = \mathrm{EPr}^{-1}$. Problem (1) was solved in a rectangular box with boundary conditions periodic in x and y. At the boundaries $z = 0,1$ we assume zero perturbations of the temperature T. Keeping in mind the chosen T_0, profile, this is equivalent to specifying the following boundary temperatures: $\widetilde{T} = T + T_0 = 1, 0$ (heating from below). For the velocity field, we assume the no-penetration condition and zero gradients of the tangential components of the field at $z = 0,1$: $V_z = \frac{\partial V_x}{\partial z} = \frac{\partial V_y}{\partial z} = 0$. This formulation of the boundary conditions guarantees that the tangential components of the viscous stress tensor and the hydrodynamic helicity are zero. A pseudospectral code (see (Orzag, 1971; Meneguzzi and Pouquet, 1989; Cattaneo et al., 2003) for more details) adapted to parallel computing using MPI (Reshetnyak, 2007) was applied to solve (1). The N^3 computational grid was used with $N = 64$.

FLUXES IN WAVE SPACE

In different fields of physics, energy transfer processes are often examined in the spectral space. Quite reasonably, hydrodynamics is one of such fields (Lesieur, 1997). The possibility of energy transfer from large to small scales is the basis of the Kolmogorov theory, in which it is postulated that there is a self-similarity area in the wave space (the so-called inertial interval) where the energy flux from one wavenumber to another is constant and dissipation as well as the work of external forces are zero (for more details of the history of the problem, see (Frisch, 1995)). According to the model, in the case of homogeneous and isotropic turbulence, the energy is transferred from larger to smaller scale vortices. For more complex systems, for example, for thermal turbulence or for magnetic-field related problems, the concept of inertial interval becomes, in the strict sense, incorrect, because the work of the forces is nonzero at almost all scales. Moreover, the energy transfer can reverse, and a so-called inverse energy cascade from small to large scales can arise (Kraichnan and Montgomery, 1980) as it happens both in the case of two-dimensional turbulence, close by its properties to rotating turbulence, and in the case of magnetic turbulence (see the theory of the α effect in the book by Krause and Rädler, 1980). It turns out that in many cases, even if forced convection is considered, a simplified representation of energy transfer as a serial transfer from scale to scale is only a rough approximation on some scale. An examination of the Fourier-mode interaction demonstrates the very complicated structure of the wave triangle and the dependence of the result on the spectrum extent (Alexakis et al., 2007). Even if we suppose a local character of the energy transfer over the spectrum and suggest that the energy is passed from a mode with a wavenumber $Q = |\mathbf{q}|$ to a mode with a wavenumber $K = |\mathbf{k}|$, and $P \sim K$, the amplitude of the third harmonic of the triad P ($\mathbf{p} + \mathbf{q} + \mathbf{k} = 0$) may be strongly different from P and Q. If $P \sim Q \sim K$, it is usually said that the triad interaction is local. If $P \ll Q$ (or $P \gg Q$), the local energy transfer is due to nonlocal interactions. Computations show that the models reproducing the spectrum with a slope of about $-5/3$, which is close to the value predicted by Kolmogorov, generally also demonstrate a strong interaction with the scale of the driving force. According to the classification suggested above, this corresponds to a nonlocal interaction and is equivalent to the deformation of small eddies by large ones.

The introduction of rotation results in a considerable reorganization of the flows both in physical and wave spaces. Although the Coriolis force does not do work by itself, the amplitude of large-scale flows can grow as conditions appear favorable for the inverse energy cascade, which was shown by direct computations (Hossain, 1994) and predicted by the theory (McComb, 1992). As a consequence, the slope of the kinetic energy spectrum also increases from $-5/3$ to -2 (Zhou, 1995; Constantin, 2002). The blocking of the energy transfer through the spectrum is responsible for this change (Zhou, 1995).

If thermal convection is also considered in the problem, the equation for temperature and buoyancy is added. In this case, conditions favorable for cyclonic convection with intense vertical velocities arise. In geodynamo studies, the problem has been properly examined in physical space. Fast rotation results in an equilibrium between the Coriolis force and the pressure gradient (the geostrophic balance) (Pedlosky, 1987; Boubnov and Golitsyn, 1995): $1_z \times \mathbf{V} \sim \nabla p$,

from which it follows that the field gradients along the rotation axis $\mathbf{z}$ are small: $\frac{\partial \mathbf{V}}{\partial z} \sim 0$.[1] Cyclones (anticyclones) arise, elongated along the axis of rotation. If we take the Earth's liquid core and reduce the amplitude of the heat sources down to the level corresponding to the convection onset, the diameter $d_c \sim E^{1/3}$ of such a cyclone will be five orders of magnitude smaller than its height. In fact, convection in the Earth's core is turbulent, and thus there exist a packet of such cyclones in the wave space. However, the estimates by the order of magnitude show that the geostrophic balance is satisfied at least for the first three to four orders in k. This is considerably above the spectral extent of the geomagnetic field and should be taken into account while constructing dynamo models.

The appearance of the Coriolis force is also important for the dynamics of energy transfer in the wave space. While earlier the nonlinear term, which was of the same order as the pressure gradient, easily transferred energy over the spectrum (for example, owing to the vortex component of the nonlinear term), the following situation became possible when the Coriolis force appeared: the pressure balances the potential component of the Coriolis force. The vortex component of the Coriolis force blocks the energy transfer by the nonlinear term. As a consequence, the spectrum becomes steeper. This is the case, at small scales $l \ll d_c$. At large scales, $l \gg d_c$, the system can be in statistical equilibrium, when dissipation is nearly zero and the energy transfer between scales is negligible.

For more details of the concept of fluxes in the wave space, see (Frisch, 1995), (Reshetnyak, 2008), and the references therein. The exchange interactions in the Fourier space can be conveniently described by partitioning the wave space into shells so that $k_i < k < k_{i+1}$, $k_{i+1}/k_i = \gamma$, is usually equal to 2. Further, we will consider the energy transfer between such shells (cascade processes). Let us decompose a field f into a sum of low and high-frequency counterparts: $f(\mathbf{r}) = f^<(\mathbf{r}) + f^>(\mathbf{r})$, where

$$f^<(\mathbf{r}) = \sum_{|k|\le K} \hat{f}_k e^{i\mathbf{kr}}, \qquad f^>(\mathbf{r}) = \sum_{|k|>K} \hat{f}_k e^{i\mathbf{kr}}, \tag{2}$$

respectively. For periodic fields f and g, we have (see (Frisch, 1995) for details):

$$\left\langle \frac{\partial f}{\partial x} \right\rangle = 0, \qquad \left\langle g \frac{\partial f}{\partial x} \right\rangle - \left\langle f \frac{\partial g}{\partial x} \right\rangle, \qquad \left\langle f^> g^< \right\rangle = 0, \tag{3}$$

where

$$\langle f(\mathbf{r}) \rangle = \mathscr{V}^{-1} \int_{\mathscr{V}} f(\mathbf{r}) \mathrm{d}\mathbf{r}^3 \tag{4}$$

stands for the averaging of the field f over the volume $\mathscr{V}$. Multiplying the Navier–Stokes equation by $\mathbf{V}^<$, leads to the equation for the mean volume of the change in the kinetic energy in a sphere with the radius K:

$$\begin{aligned} &2^{-1}\mathrm{E}\,\mathrm{Pr}^{-1}\left[\frac{\partial \left\langle V_i^< V_i^< \right\rangle}{\partial t} + \Pi(K)\right] \\ &= \mathrm{Ra}\left\langle T^< V_z^< \right\rangle - \mathrm{E}\left\langle (\nabla \omega^<)^2 \right\rangle, \end{aligned} \tag{5}$$

where the integral flux of kinetic energy from the region $k > K$ to the region $k \le K$ is given in the form

$$\Pi(K) = \left\langle V_i^< \cdot (V_j \cdot \nabla_j) V_i \right\rangle, \tag{6}$$

and the summation is implied over the repeated indices $i = 1, \ldots, 3$. It is convenient to introduce a local flux of kinetic energy T_K:

$$T_K(k) = -\frac{\partial \Pi(k)}{\partial k}, \qquad \int_{k=0}^{\infty} T_K(k) \mathrm{d}k = 0. \tag{7}$$

Then, the Navier–Stokes equation reads

$$\frac{\partial E(k)}{\partial t} T_K(k) + F_A(k) + D(k), \tag{8}$$

where $E(k) = \frac{1}{2}\frac{\partial}{\partial k}\left\langle \mathbf{V}_k^2 \right\rangle$ is the variation of the kinetic energy at the wavenumber k, $F_A(k) = \frac{\mathrm{Ra}\,\mathrm{Pr}}{\mathrm{E}} \frac{\partial}{\partial k} \left\langle T V_z^< \right\rangle$ is the work of the Archimedes force, and $D(k) = -\mathrm{Pr}\, k^2 E(k)$ is the dissipation. Relation (8) describes the total kinetic energy flux for the wavenumber k.

Similarly, for the pulsation flux T^2 we have $T_T = -\frac{\partial}{\partial k}\left[\left\langle T^< (V_i \cdot \nabla_i) T \right\rangle - \left\langle T^< V_z \right\rangle\right]$, where the second term allows for the explicit form of the temperature profile T_0. Below, we will examine only the first term in T_T.

To investigate the detailed structure of the triad mechanism, we should discuss the type of the energy equation describing the energy transfer from shells Q and P to shell K. The Navier–Stokes equation reads

$$\frac{\partial E(K)}{\partial t} = T_3^{VV} + A(K) + D(K), \tag{9}$$

where $E(K)$ and $D(K)$ have the same form as in (8), and $T_3^{VV} = \left\langle V_i(K) \cdot (V_j(P) \cdot \nabla_j) V_i(Q) \right\rangle$, $A(K) = \frac{\mathrm{Ra}\,\mathrm{Pr}}{\mathrm{E}} \left\langle T(K) V_z(K) \right\rangle$. For T^2, the expression for the flux looks as follows: $T_3^{TT} = \left\langle T(K) \cdot (V_j(P) \cdot \nabla_j) T(Q) \right\rangle$.

[1] Note that here we mean the balance of the potential component of the Coriolis force.

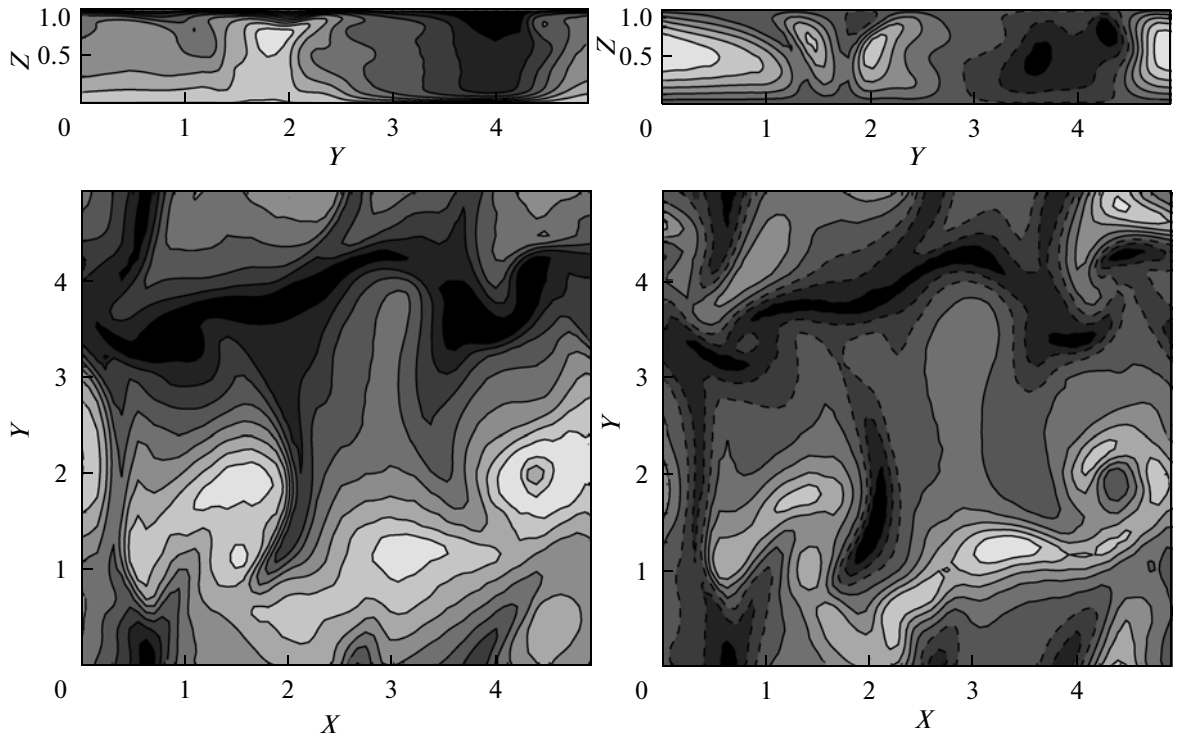

Fig. 1. Cross sections of the fields of temperature $T + T_0$ and the vertical velocity component V_z for the case without rotation (NR regime). The upper panels are for $x = 4.3$, whereas the lower panels are for $z = 0.8$. The field ranges are (0, 1), (−257, 506), and (0.03, 0.86), (−254, 572).

It is also useful to introduce the function $T_2(K,Q) = \int T_3(K,Q,P)\mathrm{d}P$. Generally speaking, the last statement needs some explanation. We can show that T_2 means the energy flux from harmonic Q to harmonic K (see the references in (Alexakis et al., 2007)). Analyzing T_2, we can estimate whether the energy transfer is local or not, but we cannot estimate the locality of the interaction itself. Examining T_3, we can completely reproduce the structure of the wave triangle and find out whether the interaction is local or not. Note also some useful properties of the function T_2: in the general case, for arbitrary periodic (or random homogeneous) nondivergent fields $\mathbf{u}(Q)$, $\mathbf{w}(K)$, and $\mathbf{V}$, we have (Alexakis et al., 2005): $T_2^{uw}(Q,K) = -T_2^{wu}(K,Q)$, where $T_2^{uw}(Q,K) = \langle u_i(K)\cdot(V_j\cdot\nabla_j)w_i(Q)\rangle$, $T_{wu}(Q,K) = \langle w_i(Q)\cdot(V_j\cdot\nabla_j)u_i(K)\rangle$, which corresponds to the equality of the energy obtained by shell K from shell Q to the energy transferred from shell Q to shell K. In the next section, we will consider the properties of the fluxes T_K, T_2 using system (1) as an example and find out how they change after the rotation is introduced.

FLOW STRUCTURE

The onset of convection in an infinite plane layer is a threshold phenomenon resulting from the increase in the Rayleigh number up to its critical value $\mathrm{Ra}^{\mathrm{cr}}$. Let us consider three convection regimes (Fig. 1):

NR: No-rotation regime (the Coriolis force is zero), $\mathrm{Ra} = 9\times10^5$, $\mathrm{Pr} = 1$, and $\mathrm{E} = 1$.

R1: Regime with rotation, $\mathrm{Ra} = 4\times10^2$, $\mathrm{Pr} = 1$, and $\mathrm{E} = 2\times10^{-5}$.

R2: Regime with rotation, $\mathrm{Ra} = 1\times10^3$, $\mathrm{Pr} = 1$, and $\mathrm{E} = 2\times10^{-5}$.

The NR regime corresponds to turbulent convection without rotation[2] with the quasi-periodic in time behavior of the kinetic energy $E_K(t)$. Note the appearance of a small-scale hydrodynamic helicity $\mathcal{H}^{\mathcal{H}} = \mathbf{V}\cdot\mathrm{rot}\mathbf{V}$. The average helicity $\overline{\mathcal{H}^{\mathcal{H}}_{\gamma}}$ is zero for the no-rotation case because no preferred direction exists. For more details, see the studies on the dynamo theory of mean fields (Moffat, 1978: Krause and Rädler, 1980;

[2] Since at the onset of convection the horizontal scales $L_x = L_y$ of the convective cell exceed its vertical scale L_z, a horizontally elongated box is usually applied. In our computations, $L_x = L_y = 5L_z \equiv 5L$.

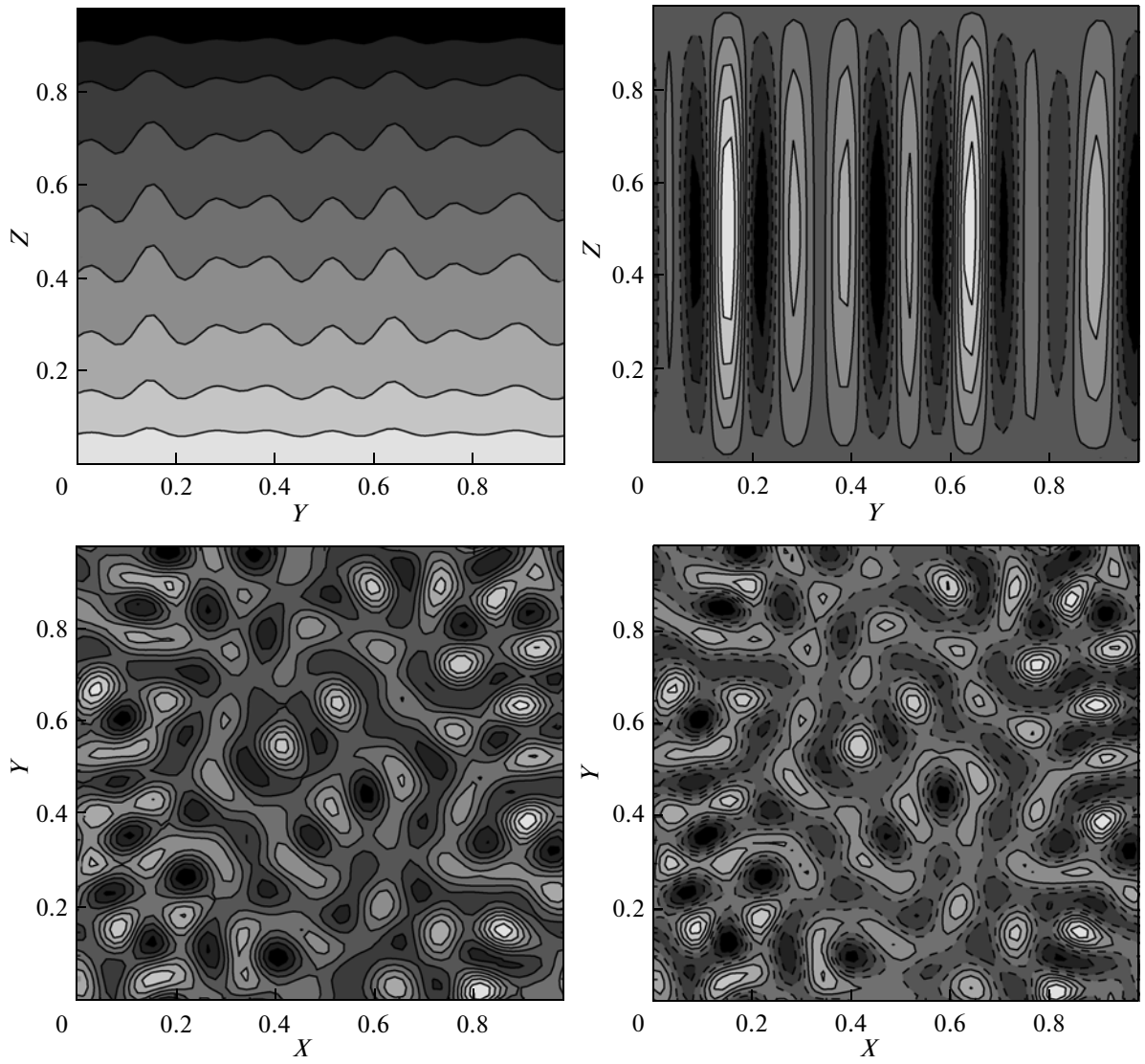

Fig. 2. Cross sections of the fields of temperature $T + T_0$ and the vertical velocity component V_z for the case with rotation (R1 regime). The upper panels are for $x = 4.3$, whereas the lower panels are for $z = 0.8$. The field ranges are (0, 1), (–88, 127), and (0.17, 0.23), (–55, 86).

Zeldovich, Ruzmaikin, and Sokoloff, 1983) and the results of direct numerical simulations (Meneguzzi and Pouquet, 1989).

Thermal convection with rotation is characterized by the appearance of a large number of vertical rotating columns (cyclones–anticyclones). Their number depends on the Ekman number as $k_c \sim \mathrm{E}^{-1/3}$ (Chandrasekhar, 1961; Busse, 1970; Jones and Roberts, 2000). For the Earth's liquid core, $\mathrm{E} \sim 10^{-15}$, this obviously makes numerical simulations with realistic values of this parameter impossible. Regimes with $\mathrm{E} = 10^{-4}$–10^{-6} (Jones, 2000) are usually accessible. The numerical experiments are aimed at obtaining an asymptotic regime and making the corresponding extrapolation to terrestrial parameters. From the linear analysis, we know that the critical Rayleigh number, related to the convection onset, depends on the Ekman number as $\mathrm{Ra}^{\mathrm{cr}} \sim \mathrm{E}^{-1/3}$. Increasing $\mathrm{Ra}^{\mathrm{cr}}$ leads to cyclonic convection, which in turn results in enhanced dissipation.

The R1 corresponds to the geostrophic state of convection near its onset threshold, which is characterized by a regular spatial structure of cyclones (Fig. 2). The increase in Ra (regime R2) leads to the disordering of cyclones, the appearance of small-scale flows in the z direction, and to a deviation from geostrophy. The amplitude of the nonlinear term becomes closer to those of the Coriolis force and the pressure gradient; the time behavior becomes more chaotic. Hydrodynamic helicity appears in both cases with rotation. It

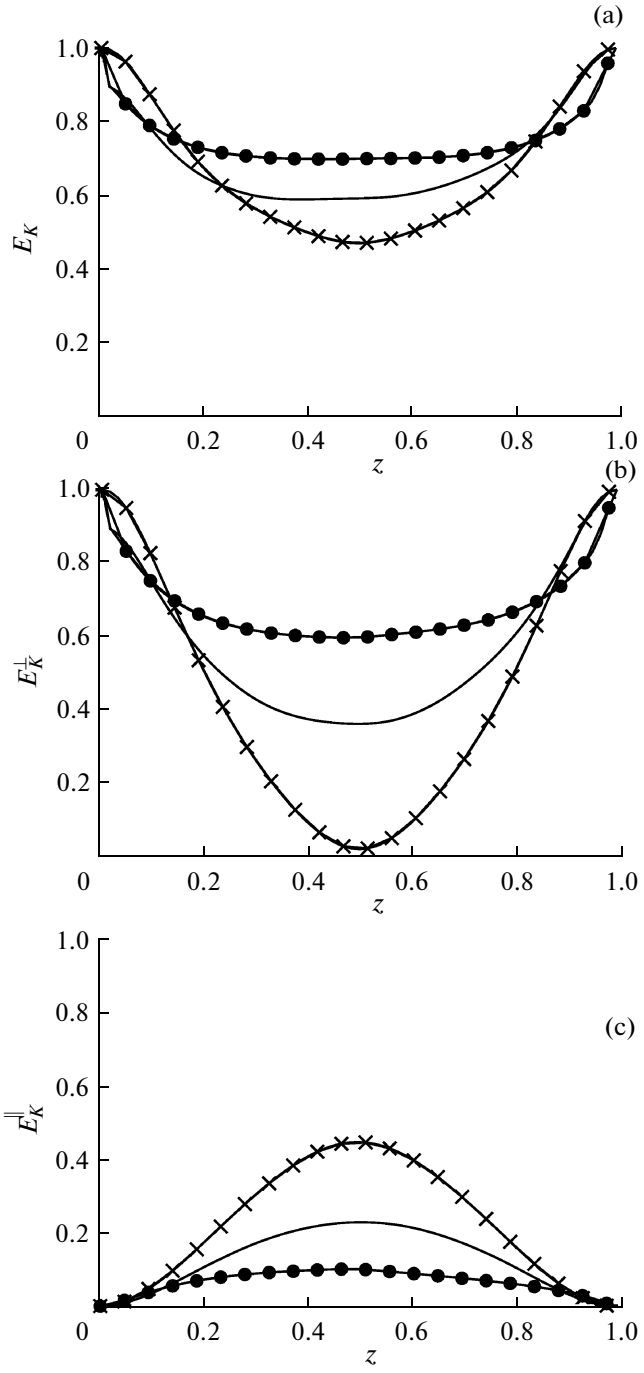

Fig. 3. The dependence of the total kinetic energy E_K (a) and transverse $E_K^{\perp}$ (b) and longitudinal $E_K^{\parallel}$ (c) energy components for the three regimes: NR (solid line), R1 (crosses), and R2 (circles). All functions are normalized by the maximum E_K.

behaves like $\mathcal{H}^{\mathcal{H}} = \langle \mathbf{V} \cdot \mathrm{rot}\mathbf{V} \rangle_{xy} \sim z - 0.5$ (averaging is made in the (x, y) plane) in the main volume. As mentioned above, $\mathcal{H}^{\mathcal{H}}$ is zero for the NR regime.

Let us consider in more detail the behavior of kinetic energy for different velocity components along the z coordinate (Fig. 3). The different behavior of the transversal $E_K^{\perp} = \left(V_x^2 + V_y^2\right)/2$ and longitudinal $E_K^{\parallel} = V_z^2/2$ energy components is related to the boundary conditions. For the NR regime, the energy components are comparable in the main volume:

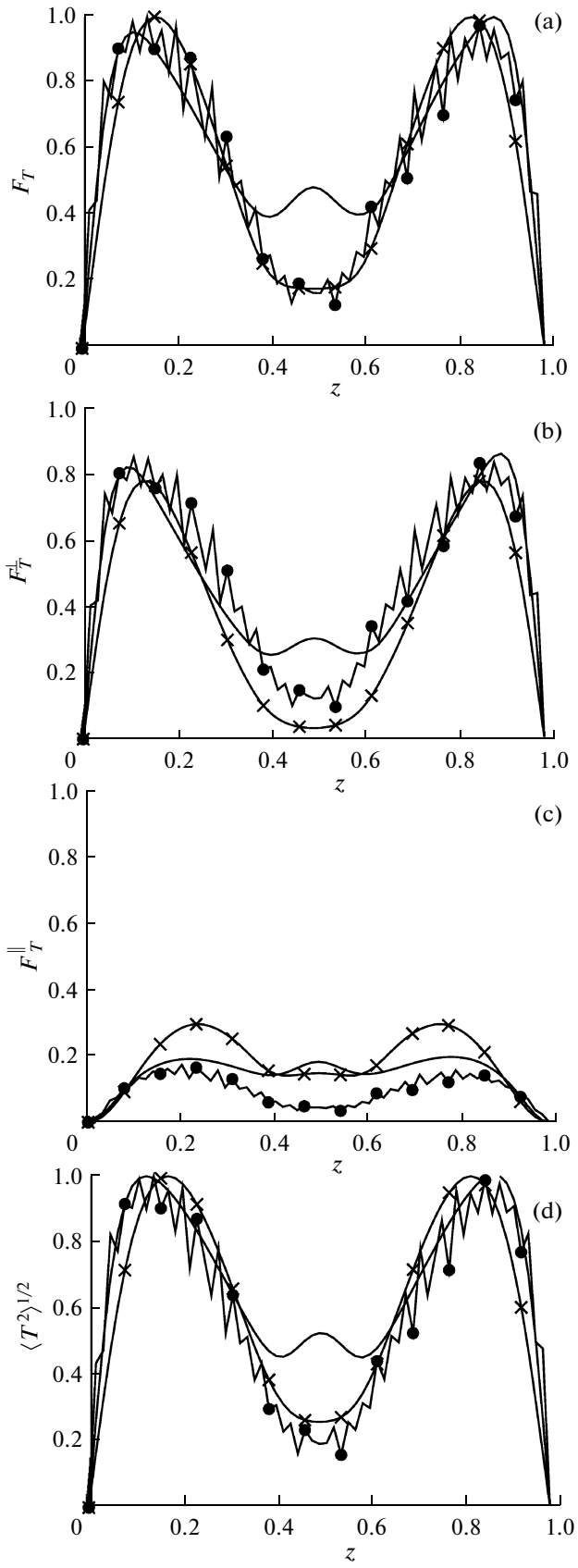

Fig. 4. The intensity of the fluxes F_T (a), $F_T^{\perp}$ (b), and $F_T^{\parallel}$ (c) and the temperature fluctuations $\langle T^2 \rangle^{1/2}$ (d) for the three regimes: NR (solid line), R1 (crosses), and R2 (circles). All functions are normalized by the maximum F_T.

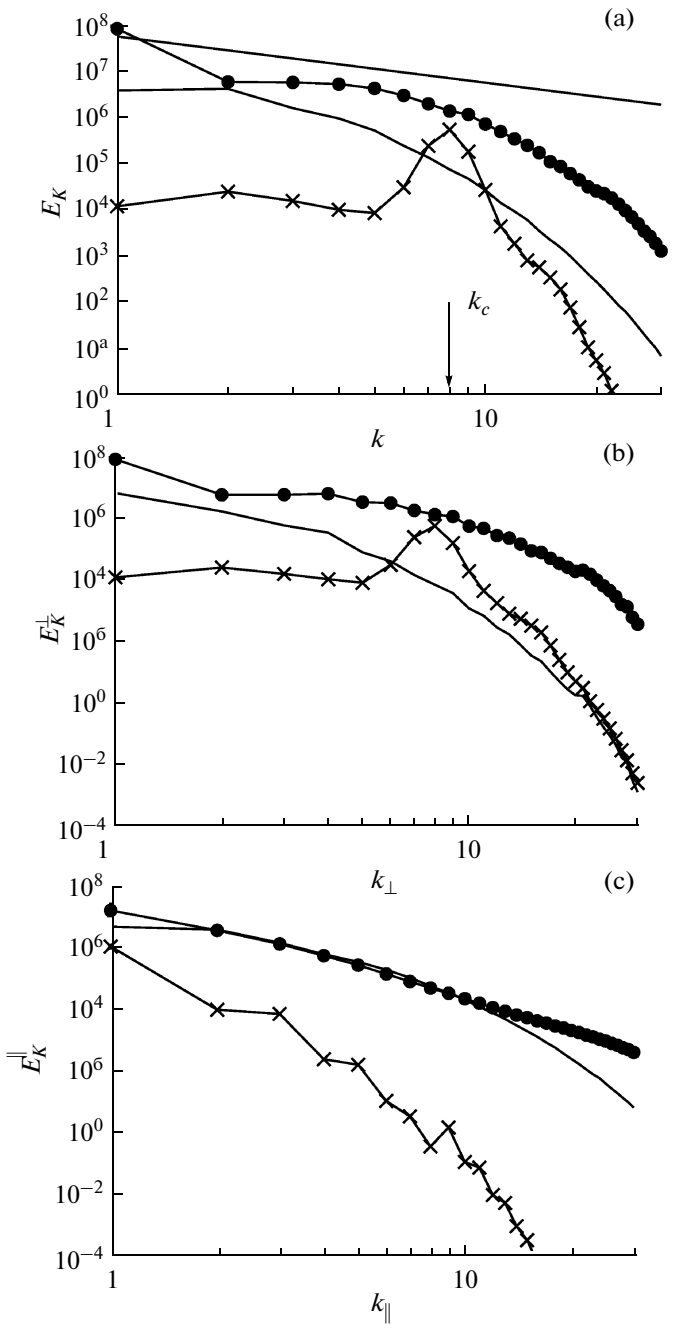

Fig. 5. The spectra of kinetic energy E_K, $E_K^\perp$, $E_K^\parallel$ as a function of (a) k, (b) $k_\perp$, and (c) $k_\parallel$ for regimes NR (solid line), R1 (crosses), and R2 (circles). The straight line corresponds to the $\sim k^{-5/3}$ Kolmogorov spectrum.

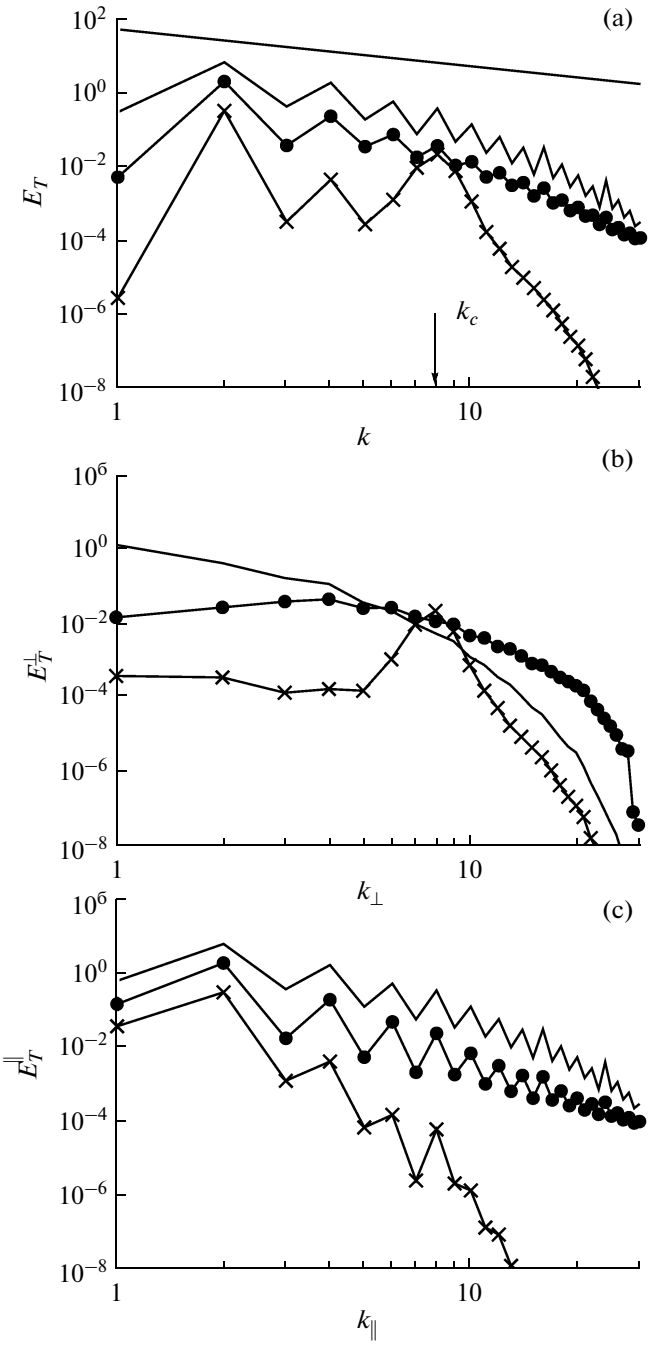

Fig. 6. The spectra of temperature fluctuations $T^2 F_T$, $E_T^\perp$, $E_T^\parallel$ as a function of (a) k, (b) $k_\perp$, and (c) $k_\parallel$ for regimes NR (solid line), R1 (crosses), and R2 (circles). The straight line corresponds to the $\sim k^{-5/3}$ Kolmogorov spectrum.

$\lambda_K^{\mathrm{NR}} \dfrac{E_K^\perp}{2E_K^\parallel}\Big|_{z=0.5} \sim 0.8$, where the factor 2 arises due to the summing over two horizontal directions. On the contrary, for R1, the sign of the rotation changes when approaching the central region and $E_K^\perp$ turns to zero: $\lambda_K^{\mathrm{R1}} \sim 0.2$. It is interesting that the increase in Ra (R2 regime) results in increased anisotropy in the entire volume: $\lambda_K^{\mathrm{R2}} \sim 10$, this means that at a sufficiently large Ra and strong rotation, the vertical fluxes of kinetic energy degenerate. First, the degeneration of the third

dimension in the three-dimensional convection during rotation was predicted by Batchelor (1953) (see also the similar degeneration due to the effect of a large-scale magnetic field (Kraichnan, 1965)). When Re increases (R2), layer structures arise at $z = 0, 1$. The last effect is associated both with the existence of the thermal boundary layer with a thickness $\delta_T \sim \mathrm{Ra}^{-1/3}$, and with the inviscid boundary conditions for V_x and V_y.

Let us consider how the anisotropy associated with the heterogeneous spatial distribution of kinetic energy affects the convective heat transfer. Figure 4 demonstrates the fluxes $F_T^{\perp}(z) = \langle |TV_x| + |TV_y| \rangle_{xy}$, $F_T^{\parallel}(z) = \langle |TV_z| \rangle_{xy}$ and $F_T = F_T^{\perp} + F_T^{\parallel}$. A specific feature of regimes with rotation is small fluxes $F_T^{\parallel}$ in the central region. This is due to the reduction of pulsations $\langle T^2 \rangle$, although the amplitude of V_z grows away from the boundaries (see Fig. 4d). The maxima of $\langle T^2 \rangle$ correspond to the boundaries of the thermal boundary layers. The corresponding anisotropy coefficients at the maxima of F_T $\lambda_T = \dfrac{F_T^{\perp}}{2F_T^{\parallel}}$ are $\lambda_T^{\mathrm{NR}} \sim 2$, $\lambda_T^{\mathrm{R1}} \sim 1$, $\lambda_T^{\mathrm{R2}} \sim 5$. In other words, rotation blocks the heat transfer along the axis of rotation at sufficiently large Ra.

SPECTRAL PROPERTIES

For all three regimes, we introduce integral, longitudinal, and transverse kinetic energy spectra: $E_K(k)$, $E_K^{\parallel}(k_{\parallel}) = \iint E_K(k_x, k_y, k_z)\mathrm{d}k_x\mathrm{d}k_y$, and $E_K^{\perp}(k_{\perp}) = \int E_K(k_x, k_y, k_z)\mathrm{d}k_z$ respectively. Here, $k_{\perp}^2 = k_x^2 + k_y^2$, $k_{\parallel} \equiv k_z$.

For the NR regime, the spectral properties of convection are close to the Kolmogorov dependence $\sim k^{-5/3}$ (Fig. 5). The behavior of the spectra $E_K^{\parallel}$ and $E_K^{\perp}$ differ only by the normalizing factor $\sim k$, which testifies to the high isotropy of the no-rotation regime. This result agrees well with the fact that the form of the convective cells at the onset of convection is close to isotropic.

The spectra of convection with rotation differ from those for the no-rotation case. The R1 regime is close to the onset of convection. The integral spectrum (upper panel) demonstrates a well-pronounced peak

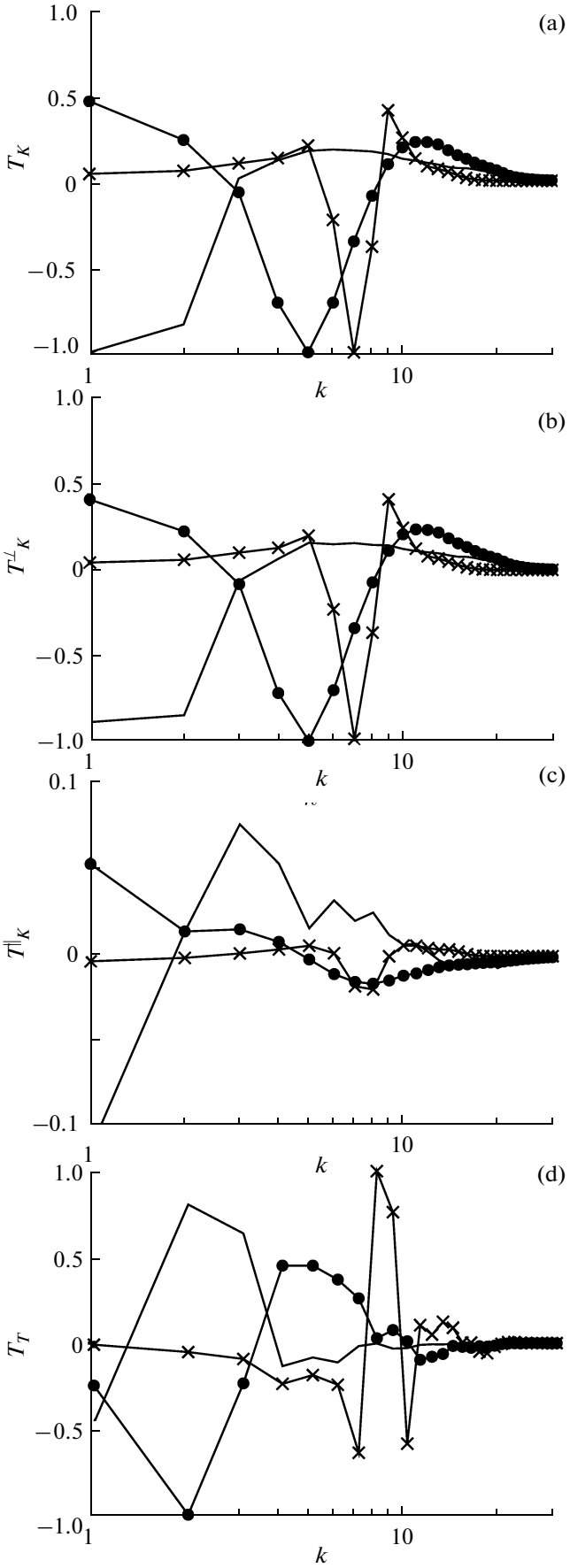

Fig. 7. The fluxes of kinetic energy T_K (a), $T_K^{\perp}$ (b), and $T_K^{\parallel}$ (c) and the temperature fluctuations T_T (d). The values are normalized by the extreme T_K for (a)–(c) and by the extreme T_T for (d).

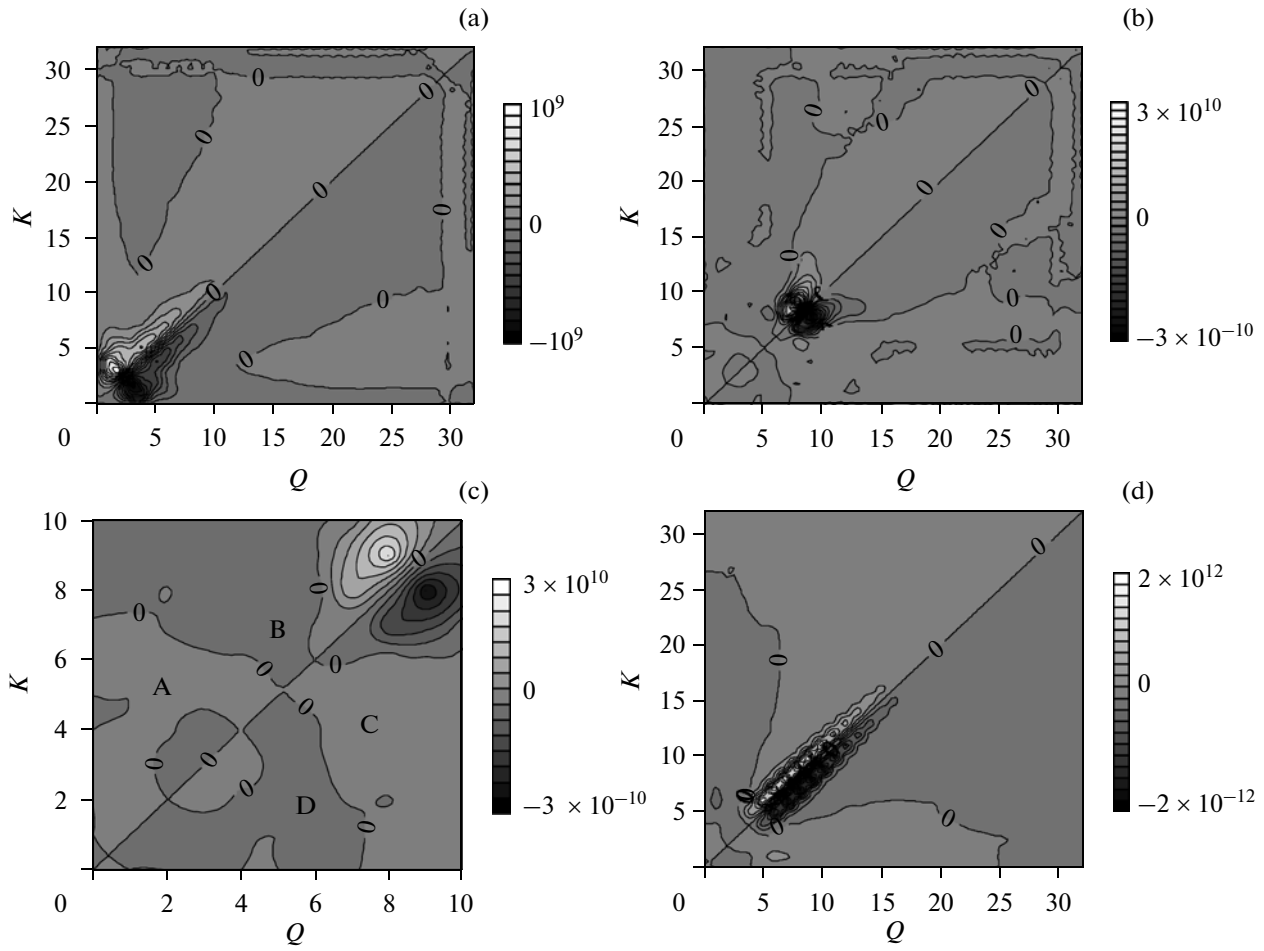

Fig. 8. The fluxes of kinetic energy $T_2^{VV}(k)$ for regimes NR (a), R1 (b), and R2 (c).

$k_c \sim 8$, corresponding to cyclonic flows. The increase in Ra (R2 regime) leads to the filling of the gap in the spectrum and the integral spectrum tends to that without rotation. The filling of the spectral gap is also observed in problems with spherical geometry (Reshetnyak, 2006) and in cascade turbulence models (Reshetnyak and Steffen, 2006).

For regime R1, the spectra $E_K^{\perp}$ and $E_K^{||}$ are strongly different: the spectrum $E_K^{||}$ does not feel the boundary $k = k_c$, whereas $k < k_c$ is close to white noise at $E_K^{\perp}$ and abruptly decays at large $k_{\perp}$. For larger Ra, $E_K^{\perp}$ approaches the Kolmogorov spectrum, whereas the transverse spectrum is still white for small $k_{\perp}$ and its slope is close to that of the spectrum without rotation at $k_{\perp} > k_c$.

Note that for regimes R1 and R2, the form of the integral spectra E_K is completely defined by the form of their transverse spectra $E_K^{\perp}$.

The spectra of temperature pulsations differ from the kinetic energy spectra by their saw-tooth character (Fig. 6). Zero boundary conditions for V_z and T are responsible for this. In all other respects, the E_T and E_K spectra are similar.

The observable similarity of the R2 and NR spectra does not mean the similarity of the intrinsic physical processes. Thus, in two-dimensional turbulence (Kraichnan and Montgomery, 1980), the kinetic energy spectrum with $\sim k^{-5/3}$ is also observed but the energy is transferred not from larger to smaller scales but in the opposite direction. The estimates for the terms for R2 (Reshetnyak, 2008) indicate that the geostrophic balance is satisfied.

Let us consider $T_K(k)$. The NR regime demonstrates the well-known pattern of the direct Kolmogorov cascade of kinetic energy (Fig. 7). For large scales $T_K < 0$, these scales are sources of energy. When moving to the infrared region, the flux changes its sign to positive; thus, the energy is consumed. The two-dimensional turbulence exhibits a mirror-symmetric

flux pattern (Kraichnan and Montgomery, 1980). In this case, the inverse energy cascade is observed instead of the direct one.

Rotation essentially changes the behavior of the energy fluxes; k_c is the energy-carrying wavenumber. For $k > k_c$, we also observe the direct energy cascade $T_K > 0$. The maximum of T_K is shifted to the right relative to the spectrum maximum and the shift is increasing with increasing Re. The situation is much more complicated for $k < k_c$ when the inverse energy cascade $T_K > 0$ is observed for small wavenumbers. At the same time, the cascade is still direct, $T_K < 0$ in most of the wavenumber range $0 < k < k_c$.

To estimate the anisotropy effects, let us decompose the T_K flux into a sum of its transverse and longitudinal parts, $T_K^{\perp}$ K and $T_K^{||}$, implying the summation in Eq. (6) over the index j for 1...2 and 3, respectively, and $i = 1...3$ for both fluxes. For all three regimes, the vertical fluxes are much smaller than the horizontal ones. Apart from this, the dependences $T_K^{||}$ are close to those of T_K. This asymmetry is associated with the following features of thermal convection. The flux $\Pi_K^{||} \sim V_z^{<}\dfrac{\partial E_K}{\partial z}$ is obviously small for geostrophic flows. It is also small for the no-rotation regimes, because the kinetic energy does not change along the vertical in the main volume and V_z is small near the boundaries. Therefore, the transverse flux Π_K contributes the most to $\Pi_K^{\perp} \sim \mathbf{V}_{\perp}^{<} \cdot \nabla_{\perp} E_K$. This asymmetry is the most significant difference between thermal convection and the homogeneous and isotropic model among all of the features that we have considered before.

It is even more complicated to analyze the fluxes of thermal energy, or, to be more exact, fluctuations of the squared perturbations of temperature T, since the distribution of $\left\langle T^2 \right\rangle^{1/2}$ is determined by the boundary layers. Therefore, we shall limit ourselves to analyzing only the integral flux T_T (see Fig. 7d). On large scales, the inverse cascade of thermal energy is observed in the NR regime. This cascade is associated with the energy flow from the boundary layer to the main volume. The effect was not observed for T_K because the inviscid boundary conditions were applied for $\mathbf{V}_{\perp}$. For regimes with rotation, the form of T_T is close to that of T_K. For a more detailed analysis of T_T, it should be considered in four separate regions corresponding to the different vertical changes of $\left\langle T^2 \right\rangle^{1/2}$ (Fig. 4d).

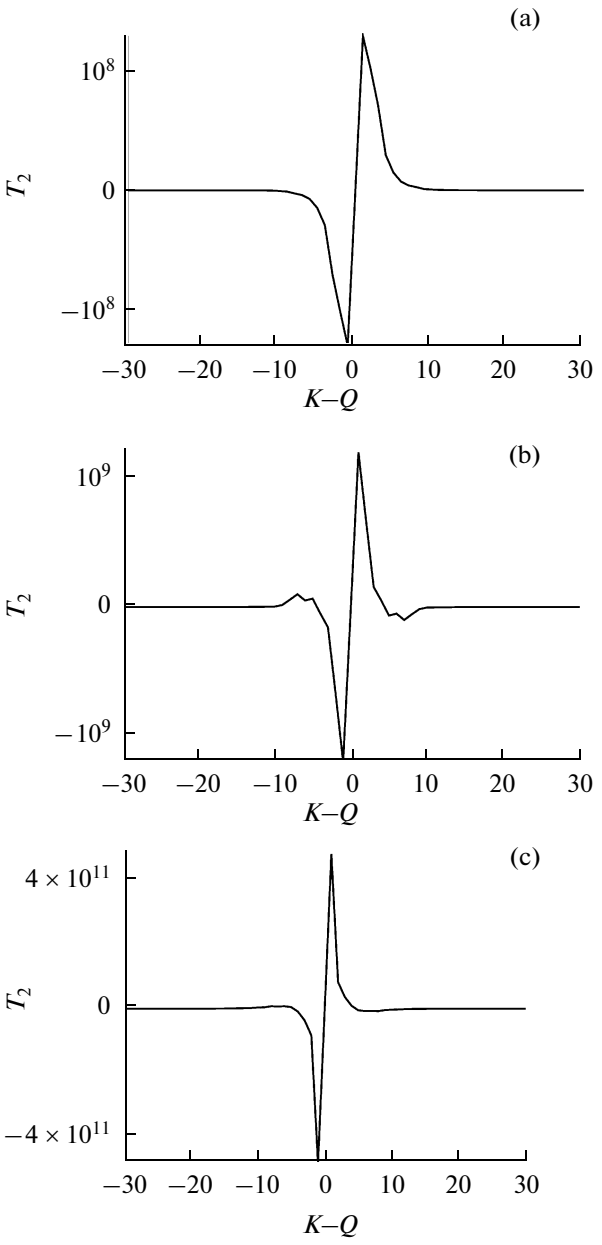

Fig. 9. The fluxes of kinetic energy $T_2^{VV}(K-Q)$ for regimes NR (a), R1 (b), and R2 (c).

THE LOCALITY OF NONLINEAR INTERACTIONS

Now let us consider the structure of triad interactions. Figure 8 presents the diagram of the kinetic energy fluxes T_2^{VV}, antisymmetric with respect to the diagonal $K = Q$, for the three regimes. On the whole, the pattern resembles the results of Alexakis et al. (2007) obtained with an imposed force: harmonics with $K > Q$ take the energy from harmonics with $K < Q$ (the direct energy cascade). The maximum energy flux corresponds to the one closest to the diagonal har-

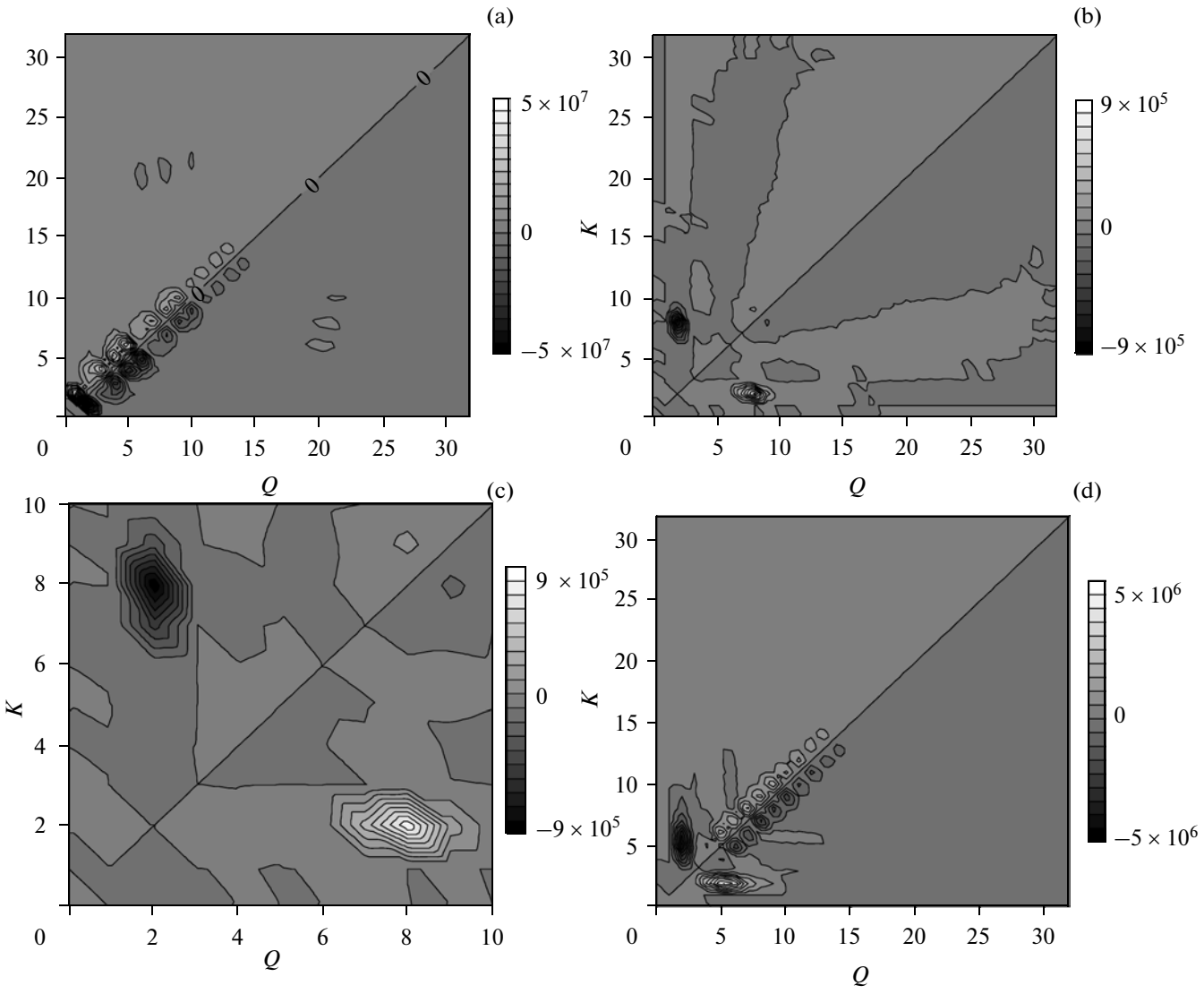

Fig. 10. The fluxes of temperature pulsations $T_2^{TT}(k)$ for regimes NR (a), R1 (b), and R2 (c).

monics with $K \sim Q$, i.e., there is a local energy transfer. Note that there are regions (for example, $Q = 5$, $K = 20$), in which a nonlocal inverse cascade of energy is observed as well (see the discussion in the Introduction); integrally, the pattern is close to the idealized Kolmogorov scenario. It is convenient to represent the diagram from Fig. 8, in the form of an integral over Q and K, as a function of K–Q (see Fig. 9). This figure clearly demonstrates the direct cascade, as well as the local interaction and local energy transfer.

The rotation changes the behavior of T_2^{VV} at $k < k_c$, leaving it unchanged in the high-frequency region $k > k_c$. Let us consider the changes in more detail. On one hand, the absolute maxima (minima) lie in the region close to k_c, this means that the energy is transferred to the region of larger k from the leading mode. On the other hand, at $k < k_c$, the energy flux drops, which corresponds to the approach of the system to the statistical equilibrium, which is also observed in Fig. 7. On a larger scale (see Fig. 8c), a finer structure is observed for small k: region A with the direct energy cascade, but with an equiprobable energy transfer both from small $Q \sim K$ and from rather large $Q \sim 4K$. Region B with the inverse energy cascade (and, like region A, with a small (about 1/10 of the absolute maximum) amplitude of energy fluxes) has an elongated strip-like form from $Q \sim K$ to $Q \sim 10K$. This corresponds to the appearance of a small negative minimum for $K > Q$ in Fig. 10.[3]

[3] We do not make any comments about the behavior of the curve for $K < Q$ (regions C and D), because this function is antisymmetric.

The increase in Ra (R2 regime) leads to the shifting of the region with the inverse energy cascade towards small Q and $K > Q$. As before, here we can speak about the existence of a state close to the equidistribution for $k < k_c$. This regime is also characterized by a longer interval in the region of $k > k_c$ with the local energy transfer and direct cascade. The relative contribution of the region with the inverse cascade becomes smaller (see Fig. 9b). At the same time, this contribution shifts to the large-scale region $k \ll k_c$. This can be interesting for geodynamo applications, where $k_c \sim 10^5$ and the region of the geomagnetic field generation (which corresponds to the range $k \sim 1$–10^3 for the state-of-the-art estimates of the magnetic Reynolds number $\mathrm{R_m} \sim 10^2$–10^3) are separated by at least several orders of magnitude.

The properties of the T_2^{TT} and T_2^{VV} diagrams are similar for NR (see Figs. 10, 11). Rotation leads to the appearance of an inverse cascade with a high degree of nonlocality in the energy transfer: the extrema in Fig. 10c are shifted with respect to the diagonal. The latter is also manifested in shifting the maxima (minima) from the point $K = Q$ in Fig. 11. It appears that the nonlocality is stronger manifested for the equation of heat transfer than for the Navier–Stokes equation (see Fig. 9). The increase in Ra leads to the reduction of nonlocality. However, as before, the boundary between the direct and inverse cascades with $k \sim k_c$ is still clearly apparent (see Fig. 10d).

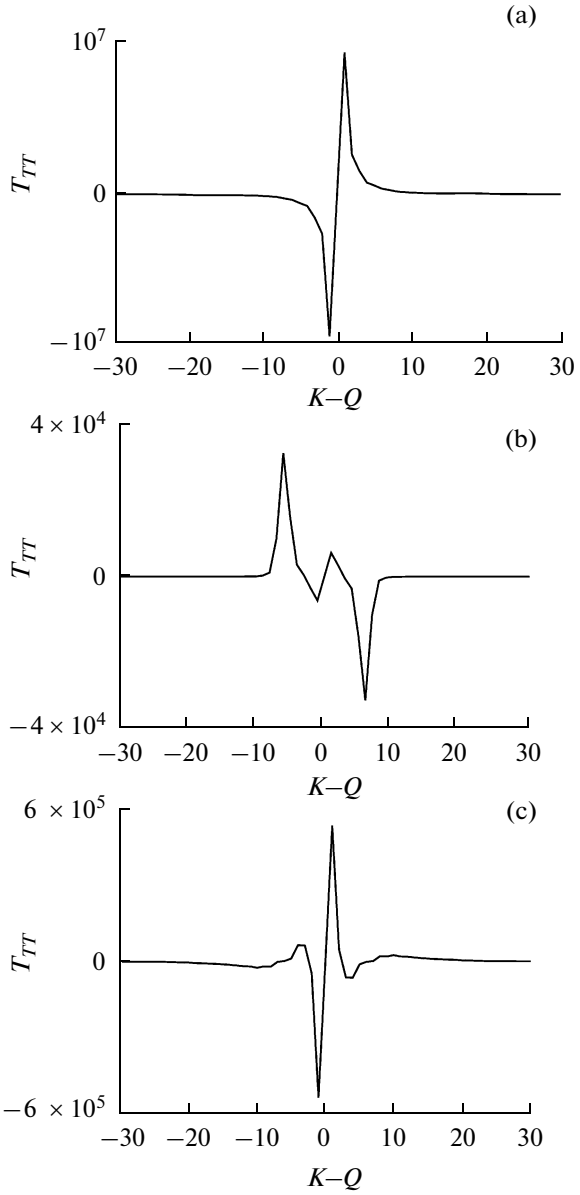

Fig. 11. The fluxes of temperature pulsations $T_2^{TT}(K-Q)$ for regimes NR (a), R1 (b), and R2 (c).

DISCUSSION

Now let us discuss how our results can be used in describing the processes in the Earth's core. It is well-known (Hunter and Riahi, 1975; Boubnov and Golitsyn, 1995) that the influence of rotation on thermal convection can be estimated by the ratio between the Rayleigh number $\widehat{\mathrm{Ra}} = \mathrm{Ra}\,\mathrm{E}^{-1}$ and the Taylor number $\mathrm{Ta} = \mathrm{E}^{-2}$. Convection is possible at $\mathrm{Ta} \ll \widehat{\mathrm{Ra}}^{3/2}$. The role of rotation is small at $\widehat{\mathrm{Ra}} \gg \mathrm{Ta}$ (*i*). At $\widehat{\mathrm{Ra}} \ll \mathrm{Ta} \ll \widehat{\mathrm{Ra}}^{4/3}$ the rotation may lead to the enhanced heat flux (*ii*) in the case of no-slip conditions (Rossby, 1969). The last effect is due to the "pressing" of the thermal boundary layer by the Ekman layer with an increasing Ta. The rotation results in weaker heat fluxes and the cessation of convection at $\widehat{\mathrm{Ra}}^{4/3} \ll \mathrm{Ta} \ll \widehat{\mathrm{Ra}}^{3/2}$ (*iii*). In the study, we focused on the behavior of fields in the main volume; therefore, we chose the inviscid boundary conditions. However, even with allowance for the inviscid boundary conditions, the increase in the heat flux is impossible in regime *ii* because the Ekman layer is thinner than the thermal boundary layer.

The estimates give $\widehat{\mathrm{Ra}}_\oplus \sim 10^{23}$, $\mathrm{Ta}_\oplus = 4 \times 10^{28}$, for the liquid core of the Earth (Christensen and Aubert, 2006). Thus, $\mathrm{Ta} < \widehat{\mathrm{Ra}}_\oplus^{4/3} = 4 \times 10^{30}$ and regime *ii* is observed. The above estimate corresponds to the case when Ra exceeds the critical value $\mathrm{Ra}^{\mathrm{cr}}$ at the excitation threshold by a factor of 5000. More modest estimates give $\mathrm{Ra} \sim 500\,\mathrm{Ra}^{\mathrm{cr}}$ (Jones, 2000). The R1 and R2 regimes, which were considered above, also belong to the range (*ii*): $\mathrm{Ta_{R1}} = \mathrm{Ta_{R2}} = 2.5 \times 10^9$, $\widehat{\mathrm{Ra}}_{\mathrm{R1}} = 2 \times 10^7$, $\widehat{\mathrm{Ra}}_{\mathrm{R2}} = 5 \times 10^7$. The, $\mathrm{Ta_{R1}} < \widehat{\mathrm{Ra}}_{\mathrm{R1}}^{4/3} = 9 \times 10^{10}$. The esti-

mates for the Nusselt number $\mathrm{Nu} = 1 + \langle V_z T \rangle$ give $\mathrm{Nu}_{\mathrm{NR}} = 5$, $\mathrm{Nu}_{\mathrm{R1}} = 1.4$, $\mathrm{Nu}_{\mathrm{R2}} = 3.9$. It is interesting that the systems with rotation exhibit the fast (as compared to nonrotating systems) growth of heat fluxes with an increasing $\widehat{\mathrm{Ra}}$. The scaling with $\mathrm{Nu} \propto \widehat{\mathrm{Ra}}^{2/7}$ is changed to the "intermediate" scaling $\mathrm{Nu} \propto \widehat{\mathrm{Ra}}^{6/5}$ (for the details of the numerical simulations, see (King et al., 2009)). Note that the faster growth of heat transfer $\mathrm{Nu} \propto \widehat{\mathrm{Ra}}^3 / \mathrm{Ta}^2$ was also observed in the experiments (Boubnov and Golitsyn, 1995). The realization of one or another scaling may depend on the selection of the boundary conditions in the horizontal direction, which is closely related to the formation of horizontal ridge structures in the cases when periodic boundary conditions are applied in numerical models. At the same time, the increase in the Reynolds number for horizontal velocities $\mathrm{Re}^{\mathrm{V}} \propto \widehat{\mathrm{Ra}}^2$ (Boubnov and Golitsyn, 1995) is close to that observed, $\frac{\mathrm{Re}^{\mathrm{V}}_{\mathrm{R1}}}{\mathrm{Re}^{\mathrm{V}}_{\mathrm{R2}}} = 8.3 \sim \left(\frac{\mathrm{Ra}_{\mathrm{R1}}}{\mathrm{Ra}_{\mathrm{R2}}}\right)^2 = 6.2$.

Even for relatively large amplitudes of heat sources, the system behaves differently depending on the position in the wave space relative to the leading mode k_c. A small inverse energy cascade is observed for modes with $k < k_c$, the system approaches the static equilibrium, and the interaction becomes nonlocal. Coherent structures appear which are typical of the two-dimensional turbulence (Tabeling, 2002). The energy cascade is direct for modes with $k > k_c$; however, nonlocal energy transfer from small $k \sim k_c$ may be observed. The triad mechanism for the heat transfer equation demonstrates the appearance of the inverse energy cascade even more efficiently than the Navier–Stokes equation does.

The approaches considered above demonstrate the diversity of the interactions between different modes in the system without any magnetic field, which is rather simple as compared to the general dynamo problem. Such an analysis can be useful in developing new models with turbulent transfer coefficients in order to reach an agreement between the results of direct simulations and the fluxes at scales exceeding the scale of averaging d_a. Only such step-by-step comparisons can guarantee the correctness of the introduced semiempirical turbulence model. The reproduction of the inverse cascade at $d_c < d_a$ is a nontrivial problem.

REFERENCES

Alexakis, A., Mininni, P.D., and Pouquet, A. Shell to Shell Energy Transfer in MHD. I. Steady State Turbulence, *Phys. Rev.,* 2005, vol. E72, pp. 046301–046309.

Alexakis, A., Mininni, P.D., and Pouquet, A., Turbulent Cascades, Transfer, and Scale Interactions in Magnetohydrodynamics,*New J. Phys.,* 2007, vol. 298, no. 9, pp. 1–20.

Batchelor, G.K., *The Theory of Homogeneous Turbulence,* Cambridge: Cambridge Univ. Press, 1953.

Boubnov, B.M. and Golitsyn, G.S., *Convection in Rotating Fluids*, London: Kluwer, 1995.

Busse, F.H., Thermal Instabilities in Rapidly Rotating Systems, *J. Fluid Mech.*, 1970, vol. 44, pp. 441–460.

Cattaneo, F., Emonet, T., and Weis, N., On the Interaction between Convection and Magnetic Fields, *Astrophys. J.*, 2003, vol. 588, pp. 1183–1198.

Chandrasekhar, S., *Hydrodynamics and Hydromagnetic Stability*, New York: Dover, 1981.

Christensen, U.R., Olson, P., and Glatzmaier, G.A., Numerical Modeling of the Geodynamo: A Systematic Parameter Study, *Geophys. J. Int.*, 1999, vol. 138, pp. 393–409.

Christensen, U.R. and Aubert, J., Scaling Properties of Convection-Driven Dynamos in Rotating Spherical Shells and Application to Planetary Magnetic Fields, *Geophys. J. Int.*, 2006, vol. 166, pp. 97–114.

Constantin, P., Energy Spectrum of Quasigeostrophic Turbulence, *Phys. Rev. Lett.*, 2002, vol. 89, no. 18, pp. 184501-1–184501-4.

Frisch, U., *Turbulence: The Legacy of A.N. Kolmogorov*, Cambridge: Cambridge Univ. Press, 1995.

Glatzmaier, G.A. and Roberts, P.H., A Three-Dimensional Convective Dynamo Solution with Rotating and Finitely Conducting Inner Core and Mantle, *Phys. Earth and Planet. Inter.*, 1995, vol. 91, pp. 63–75.

Hossain, M., Reduction in the Dimensionality of Turbulence Due to a Strong Rotation, *Phys. Fluids*, 1994, vol. 6, no. 4, pp. 1077–1080.

Hunter, C. and Riahi, N., Nonlinear Convection in a Rotating Fluid, *J. Fluid Mech.,* 1975, vol. 72, pp. 433–454.

Jones, C.A. and Roberts, P.H. Convection Driven Dynamos in a Rotating Plane Layer, *J. Fluid Mech.,* 2000, vol. 404, pp. 311–343.

Jones, C.A., Convection-Driven Geodynamo Models, *Phil. Trans. R. Soc. London*, 2000, vol. A358, pp. 873–897.

King, E.M., Stellmach, S., Noir, J., Hansen, U., and Aurnou, J.M. Boundary Layer Control of Rotating Convection System, *Nature*, 2009, vol. 457, pp. 301–304.

Kraichnan, R.H., Inertial-Range Spectrum of Hydromagnetic Turbulence, *Phys. Fluids,* 1965, vol. 8, pp. 1385–1387.

Kraichnan, R.H. and Montgomery, D., Two-Dimensional Turbulence, *Rep. Prog. Phys.*, 1980, vol. 43, pp. 547–619.

Krause, F. and Rädler, K.-H., *Mean Field Magnetohydrodynamics and Dynamo Theory*, Berlin: Akademie-Verlag, 1980.

Lesieur, M., *Turbulence in Fluids*, London: Kluwer, 1997.

McComb, W.D., *The Physics of Fluid Turbulence*, Oxford: Clarendon, 1992.

Meneguzzi, M. and Pouquet, A., Turbulent Dynamos Driven by Convection, *J.Fluid Mech.*, 1989, vol. 205, pp. 297–318.

Moffatt, H.K., *Magnetic Field Generation in Electrically Conducting Fluids*, Cambridge: Cambridge Univ. Press, 1978.

Orszag, S.A., Numerical Simulation of Incompressible Flows Within Simple Boundaries. I. Galerkin (Spectral) Representations, *Stud. Appl. Math.*, 1971, vol. L, no. 51, pp. 293–327.

Pedlosky, J., *Geophysical Fluid Dynamics,* New York: Springer, 1987.

Reshetnyak, M. and Steffen, B., Shell Models in Rapidly Rotating Dynamo Systems, *Num. Meth. and Programm.*, 2006, vol. 7, pp. 85–92 (http://num-meth.srcc. msu.su/english/zhurnal/tom_2006/v7r110.html).

Reshetnyak, M.Yu., Hydrodynamic Helicity in Boussinesq-Type Models of the Geodynamo, *Fiz. Zemli*, 2006, no. 6, pp. 3–13 [*Izvestiya. Phys. Solid Earth* (Engl. Transl.), vol. 42, no. 6, pp. 449–459].

Reshetnyak, M.Yu., Thermal Convection and the Dynamo during Rapid Rotation, *Fiz. Zemli,* 2007, no. 8, pp. 23–32 [*Izvestiya. Phys. Solid Earth* (Engl. Transl.), vol. 43, no. 8, p. 642]

Reshetnyak, M.Yu., Certain Spectral Properties of Cyclonic Turbulence in the Earth's Liquid Core, *Geomagn. Aeron.,* 2008, vol. 48, no. 3, pp. 416–423 [*Geomagn. Aeron.* (Engl. Transl.), vol. 48, no. 3, p. 400].

Rossby, H.T., A Study of Bernard Convection with and without Rotation, *J. Fluid Mech.*, 1969, vol. 36, pp. 309–337.

Stanley, S. and Bloxham, J., Convective-Region Geometry as the Cause of Uranus' and Neptune's Unusual Magnetic Fields, *Letters to Nature,* 2004, vol. 428, pp. 151–153.

Tabeling, P., Two-Dimensional Turbulence: A Physicist Approach, *Phys. Rep.,* 2002, vol. 362, pp. 1–62.

Zeldovich, Ya.B., Ruzmaikin, A.A.,and Sokoloff, D.D., *Magnetic Fields in Astrophysics,* New York: Gordon and Breach, 1983.

Zharkov, V.N., *Geofizicheskie issledovaniya planet i sputnikov* (Geophysical Studies of Planets and Satellites), Moscow: OIFZ RAN, 2003.

Zhou, Y., A Phenomenological Treatment of Rotating Turbulence, *Phys. Fluids*, 1995, vol. 7, no. 8, pp. 2092–2094.